Am J Physiol Gastrointest Liver Physiol 320: G768–G779, 2021.
First published March 3, 2021; doi:10.1152/ajpgi.00047.2021

american physiological society

AMERICAN JOURNAL OF PHYSIOLOGY
GASTROINTESTINAL AND LIVER PHYSIOLOGY

RESEARCH ARTICLE

Evidence of enteric angiopathy and neuromuscular hypoxia in patients with mitochondrial neurogastrointestinal encephalomyopathy

Elisa Boschetti,[1,2] Roberto D'Angelo,[3] Maria Lucia Tardio,[4] Roberta Costa,[1] Carla Giordano,[5] Anna Accarino,[6] Carolina Malagelada,[6] Paolo Clavenzani,[7] Vitaliano Tugnoli,[1] Giacomo Caio,[8] Valeria Righi,[9] Caterina Garone,[2] Antonietta D'Errico,[4] Giovanna Cenacchi,[1] Maria Teresa Dotti,[10] Vincenzo Stanghellini,[2] Catia Sternini,[11] Loris Pironi,[2] Rita Rinaldi,[3] Valerio Carelli,[1,12] and Roberto De Giorgio[8]

[1]*Department of Biomedical and Neuromotor Sciences, University of Bologna, Bologna, Italy;* [2]*Department of Medical and Surgical Sciences, University of Bologna, Bologna, Italy;* [3]*IRCCS Istituto delle Scienze Neurologiche di Bologna, UOC interaziendale Clinica Neurologica Metropolitana (NeuroMet), Neurologia AOU S. Orsola-Malpighi, Bologna, Italy;* [4]*IRCCS St. Orsola-Malpighi Hospital, Bologna, Italy;* [5]*Department of Medico-Surgical Sciences and Biotechnologies, University "La Sapienza", Roma, Italy;* [6]*Digestive System Research Unit, University Hospital Vall d'Hebron; Centro de Investigación Biomédica en Red de Enfermedades Hepáticas y Digestivas (CIBEREHD); Departament de Medicina, Universitat Autònoma de Barcelona, Barcelona, Spain;* [7]*Department of Veterinary Medical Sciences, University of Bologna, Bologna, Italy;* [8]*Department of Morphology, Surgery and Experimental Medicine, University of Ferrara, Ferrara, Italy;* [9]*Department of Life Quality Studies, University of Bologna, Bologna, Italy;* [10]*Department of Medical, Surgical and Neurological Sciences, University of Siena, Siena, Italy;* [11]*Digestive-Disease-Division, Departments of Medicine and Neurobiology, David Geffen School of Medicine, University of California Los Angeles (UCLA), Los Angeles, California; and* [12]*IRCCS Istituto delle Scienze Neurologiche di Bologna, Bologna, Italy*

Abstract

Mitochondrial neurogastrointestinal encephalomyopathy (MNGIE) is a rare autosomal recessive disease caused by thymidine phosphorylase (TP) enzyme defect. As gastrointestinal changes do not revert in patients undergone TP replacement therapy, one can postulate that other unexplored mechanisms contribute to MNGIE pathophysiology. Hence, we focused on the local TP angiogenic potential that has never been considered in MNGIE. In this study, we investigated the enteric submucosal microvasculature and the effect of hypoxia on fibrosis and enteric neurons density in jejunal full-thickness biopsies collected from patients with MNGIE. Orcein staining was used to count blood vessels based on their size. Fibrosis was assessed using the Sirius Red and Fast Green method. Hypoxia and neoangiogenesis were determined via hypoxia-inducible-factor-1α (HIF-1α) and vascular endothelial cell growth factor (VEGF) protein expression, respectively. Neuron-specific enolase was used to label enteric neurons. Compared with controls, patients with MNGIE showed a decreased area of vascular tissue, but a twofold increase of submucosal vessels/mm^2 with increased small size and decreased medium and large size vessels. VEGF positive vessels, fibrosis index, and HIF-1α protein expression were increased, whereas there was a diminished thickness of the longitudinal muscle layer with an increased interganglionic distance and reduced number of myenteric neurons. We demonstrated the occurrence of an angiopathy in the GI tract of patients with MNGIE. Neoangiogenetic changes, as detected by the abundance of small size vessels in the jejunal submucosa, along with hypoxia provide a morphological basis to explain neuromuscular alterations, vasculature breakdown, and ischemic abnormalities in MNGIE.

NEW & NOTEWORTHY Mitochondrial neurogastrointestinal encephalomyopathy (MNGIE) is characterized by a genetically driven defect of thymidine phosphorylase, a multitask enzyme playing a role also in angiogenesis. Indeed, major gastrointestinal bleedings are life-threatening complications of MNGIE. Thus, we focused on jejunal submucosal vasculature and showed intestinal microangiopathy as a novel feature occurring in this disease. Notably, vascular changes were associated with neuromuscular abnormalities, which may explain gut dysfunction and help to develop future therapeutic approaches in MNGIE.

angiogenesis; fibrosis; gastrointestinal bleeding; platelet-derived endothelial cell growth factor 1; submucosal vessels

Correspondence: E. Boschetti (elisa.boschetti@unibo.it).
Submitted 3 February 2021 / Revised 22 February 2021 / Accepted 23 February 2021

INTRODUCTION

Mitochondrial neurogastrointestinal encephalomyopathy (MNGIE) is a rare autosomal recessive disease caused by *TYMP* mutations, leading to a defective thymidine phosphorylase (TP) (1–3). This results in a toxic accumulation of nucleosides and mitochondrial DNA (mtDNA) abnormalities damaging various tissues, including the gastrointestinal (GI) tract. Patients with MNGIE show severe GI dysmotility and alterations of many organs, including brain and skeletal muscles, ultimately leading to a poor quality of life and death (2,3). Permanent replacement of TP is the best life-saving approach to stably reduce nucleoside imbalance, improve skeletal muscle tone and recover walking ability, re-establish oral feeding, and, therefore, ameliorate the overall patients' quality of life. Several therapeutical approaches have been developed to improve symptoms in patients with MNGIE. These include allogeneic hematopoietic stem cell (AHSCT) and liver transplantation (LT) that are effective in inducing biochemical and clinical improvement (4, 5). However, the follow-up of patients who have undergone AHSCT (5–7) or LT (4, 8–10) showed that some alterations, such as GI abnormalities including malabsorption and bleeding, along with diffuse brain leukoencephalopathy, never revert. These findings suggest that some other factors play a key role in permanent tissue abnormalities of patients with MNGIE.

TP is also known as platelet-derived endothelial cell growth factor, involved in physiological and pathological angiogenesis (11). TP converts thymidine plus phosphate in thymine and 2-deoxy-D-ribose-1-phosphate (dRP). In vitro and in vivo experiments demonstrated that dRP (and not TP enzyme activity) is the chemotactic agent that induces the endothelial progenitor cells to form/repair blood vessels (12). In particular, the release of dRP in the area of vascular injury is likely to promote endothelial cell migration from intact neighboring regions (12). The defective TP does not allow the critical conversion from thymidine plus phosphate to thymine and dRP in native MNGIE organs even in those patients who are treated with AHSCT or LT. As dRP needs to be locally released to exert its angiogenic properties (13), our working hypothesis is that this mechanism might contribute to the vascular abnormalities in tissues of patients with MNGIE, as emerged by previous studies documenting micro-angiopatic changes characterized by mtDNA depletion and metabolic impairment of the vessel wall cellular components (7, 14,15). We reasoned that vasculature abnormalities, as well as an associated impaired vascular permeability, may provide a basis to explain why key GI symptoms and brain leukoencephalopathy still persist following TP replacement therapy. Although leukoencephalopathy seems to remain asymptomatic over time, the irreversible GI abnormalities in MNGIE can be fatal. Indeed, there have been case reports of patients with MNGIE who have received AHSCT or LT who died of GI complications such as perforation or bleeding 1–3 yr later regardless of whether they suffered GI symptoms before these procedures (6, 10).

The aim of our research was to test the hypothesis that alterations of the GI vascular system in patients with MNGIE represent a possible mechanism underlying GI complications by providing a morphological and morphometrical analysis of the GI vascular tissue in full-thickness jejunal biopsies of patients with MNGIE compared with GI asymptomatic controls. Along with a qualitative assessment of the GI tissue, we measured the total area of submucosa occupied by vascular tissue, the number of vessels supplying the submucosa, their size, and percentage of each vessel size. Because of the absence of TP in MNGIE, we analyzed the localization and expression of the vascular endothelial cell growth factor (VEGF), which is known to play a contributory role in small vessel formation. Finally, the protein distribution and expression of hypoxia-inducible factor (HIF)-1α, the localization and amount of fibrosis and the number of enteric neurons were measured as an outcome of hypoxic phenomena.

METHODS

Patients

The study includes n = 5 patients with biochemically and genetically proven diagnosis of MNGIE (1 female and 4 males; age range: 20–38 yr) and n = 9 controls without symptoms suggestive of GI impairment who underwent abdominal surgery for noncomplicated GI tumors (4 females and 5 males; age range: 47–71 yr). Full-thickness biopsies (5 × 1 cm) of the jejunum were obtained from all patients and controls during abdominal surgery or laparoscopy. Control group biopsies were collected from jejunal tissue adjacent to the GI tumors, which did not show macroscopic abnormalities. Subsequent histological analysis confirmed the lack of microscopic abnormalities in control tissues. Specimens were fixed overnight in 10% formalin, embedded in paraffin and sectioned at 5 or 10 μm according to standard protocol (16). A snap frozen (−80°C) sample (1 × 1 cm) was collected in 5 controls and 2 patients with MNGIE.

Ethics Approval and Consent to Participate

The study protocol was approved by the Ethics Committee of St. Orsola-Malpighi Hospital of Bologna, Italy Protocol No. 50/2012/O/Sper (EM/146/2014/O). All subject (patients and controls) gave written informed consent to participate.

Orcein Staining

Tissue sections (10 μm) from each subject were deparaffinized in xylene and rehydrated through graded ethanol. Tissue sections were incubated 1 h with a solution containing 1% orcein, 70% ethanol, and 0.6 mL HCl. After being washed in distilled water, tissue sections were placed for 30 s in 95% ethanol, then for 30 min in a 100% ethanol solution to allow the elastic fibers to assume the typical black-brown color. To remove staining from nonelastic fibers, sections were treated with a solution containing 70% ethanol and 1% HCl for 5 min. After dehydration was completed, tissue sections were cover-slipped using mounting medium.

Small Vessels Quantitative Analysis

Orcein-stained sections were used to measure the vascular area (i.e., area of tissue occupied by blood vessels within the submucosa) and count the number of vessels detectable in the jejunal submucosa. In each section, all consecutive fields representative of the submucosal layer (at least 10 fields/

section; 3 nonconsecutive sections/patient or control) were captured using a Nikon DXM1200 digital camera (Nikon, Tokyo, Japan) mounted on a LEICA DM LB (Leica, Mannheim, Germany) light transmission microscope at a ×100 final magnification. Acquired images were evaluated with the Automatic Camera Tamer (ACT)-1 dedicated software (Nikon, Tokyo, Japan). For each control and patient section, the total area occupied by vessels was calculated in relation to the total area of the submucosa (expressed as ratio). The number of vessels was calculated on mm^2 of submucosa. The diameter of each analyzed vessel was assessed using ImageJ 1.48 V free software. To standardize the quantitative analysis, the largest diameter of asymmetrical vessels has always been considered in both controls and patients with MNGIE. Blood vessels were then subdivided into four categories, according to their diameter: >301; 300–101; 100–51; and <50 μm. In each subject (either control or MNGIE), the number of blood vessels per each category has been reported as a percentage of the total number of vessels.

Assessment of Tissue Fibrosis

The quantification of fibrosis was performed directly on formalin-fixed and paraffin-embedded tissue sections using the Sirius Red (that binds to all types of collagen)/Fast Green (for noncollagenous proteins) Staining kit (Condrex Redmond, WA). Briefly, n = 3 nonconsecutive tissue sections for each subject were deparaffinized and incubated 30 min with the Sirius red/fast green staining solution mix. After being washed with distilled water, images were captured using the previously described image acquisition system at different magnifications for a qualitative assessment. Sirius red/fast green dye was extracted on each stained section using 1 mL of dye extraction buffer included in the kit. The eluted dye solution was collected in plastic cuvette and analyzed with a 350-UV-Vis spectrophotometer (Thermo Fisher Scientific, Rockford, IL) at λ = 540 nm (fast green) and λ = 605 nm (Sirius red). Fibrosis was estimated using the ratio between collagenous and noncollagenous protein (expressed as μg/section) according to the following two formulas, respectively:

$$\text{Collagenous protein}\left(\frac{\mu g}{\text{section}}\right) = \frac{[\text{OD 540 value} - (\text{OD 605 value} \times 0.291)]}{\text{color equivalence of noncollagenous protein at OD 540 } (= 0.0378)} \quad (1)$$

and

$$\text{Noncollagenous proteins}\left(\frac{\mu g}{\text{section}}\right) = \frac{\text{OD 605 value}}{\text{color equivalence of collagenous protein at OD 605 } (= 0.00204)}. \quad (2)$$

The average obtained from control group has been used as calibrator (unitary value). For an appropriate calculation of the collagen amount, the OD 540 value was corrected by subtracting the contribution of fast green at 540 nm corresponding to 29.1% of the OD 605 value.

Longitudinal Muscle Layer Thickness

Sirius red/fast green-stained sections were also used to measure the longitudinal muscle thickness using ImageJ 1.48 V software. For each patient and control, the final value has been obtained using the average of six measurements per section, in random (nonoverlapping) fields containing the muscular longitudinal layer. These measurements were performed on three nonconsecutive sections.

VEGF, HIF-1α, and Neuron-Specific Enolase Immunostaining

Paraffin-embedded jejunal sections (5 μm) were rehydrated and antigen retrieval was performed by heating sections for 25 min at 90°C in a water bath in the presence of 10 mmol/L sodium citrate buffer pH 6.0. Sections were treated with an endogenous peroxidase blocking kit (Gene Tex, Aachen, Germany). Immunostaining was performed using a commercial kit (Millipore, Milan, Italy) following the manufacturer's instructions. Mouse monoclonal anti-VEGF (C-1:sc-7269; dilution: 0.02 μg/μL) and anti-HIF-1α (sc-13515; dilution: 0.02 μg/μL) (Santa Cruz Biotechnology, Dallas, TX) were used to label vessels and tissue and/or cells in hypoxic condition, respectively. The neuron-specific enolase (NSE) antibody (rabbit PA1-28217; dilution 1:1; Thermo Fisher Scientific, Rockford, IL) was used to label myenteric and submucosal neurons. The goat anti-mouse or anti-rabbit biotinylated secondary antibodies (dilution 1:1) were used as provided by the immunostaining kit (Millipore, Milan, Italy). The specificity of VEGF and HIF-1α antibodies has been determined with Western blotting (WB) experiments.

WB Detection of VEGF and HIF-1α Proteins

Total proteins were extracted from 0.5 g of each jejunal sample from n = 5 controls and n = 2 patients with MNGIE using TPER tissue protein extraction reagent in the presence of protease inhibitor cocktail (Thermo Fisher Scientific, Rockford, IL). Total protein fractions were quantified using a NanoDrop 2000 spectrophotometer and stored at −80°C. For WB analysis, 100 μg of total proteins were diluted (vol/vol) in homemade Laemmli sample buffer pH 6.8 (4% SDS; 20% glycerol; 120 mM Tris-Cl; bromophenol blue 0.02%) and boiled 10 min before loading onto gel. Proteins were separated using 10% SDS-PAGE and transferred onto nitrocellulose membrane overnight at 12 mV. Membranes were blocked with a buffer containing 5% fat-free milk and then incubated overnight at 4°C with VEGF or HIF-1α antibodies at 1:200 dilution. Membranes were washed three times in phosphate Tris buffer saline (100 mM Tris HCl, 1.5 M NaCl, 0.5% Tween-20, pH 8.3) and incubated with the specific horseradish peroxidase (HRP)-conjugated goat anti-mouse (A4416) or goat anti-rabbit (A6154) secondary antibodies (Millipore, Milan, Italy) diluted 1:5,000 for 2 h at room temperature. Immunoreactive bands were visualized by ECL Western Blotting Substrate (Thermo Fisher Scientific) on a C-DiGit Blot Scanner system and quantified by the dedicated software Image Studio Software v. 3.1.4 (both LI-COR, Bad Homburg, Germany). Each detected protein was normalized using the intensity of the reference proteins, that is, GAPDH (mouse monoclonal anti-GAPDH; clone 6C5 ab8245; Abcam, Cambridge, UK) or VINCULIN (rabbit polyclonal anti-vinculin antibody GTX113294; GeneTex, Inc., San Antonio, TX) 1:1,000. GAPDH proteins were detected on the same membrane following stripping with Restore Plus Western Blot

Stripping Buffer (Thermo Fisher Scientific). Each assay was conducted in duplicate on separate membranes.

Neuronal Cell Count and Interganglionic Distance

Enteric NSE immunoreactive neurons per ganglion and myenteric interganglionic distance were assessed as previously published (17). Briefly, the ganglia were counted (>5 ganglia/section) scanning with the microscope from left toward the right side of each section. With this procedure the distances between ganglia and the number of neurons per ganglion were assessed. At least n = 3 random jejunal cross sections from one specimen per patient with MNGIE and control were examined. Images (×100) were captured and the distance between consecutive ganglia was calculated using the ImageJ 1.48 V software using a 300-μm cut-off to define the arbitrary ganglionic unit (17).

Statistical Analysis

Since MNGIE is an extremely rare disorder and based on the surgical full-thickness specimens, the number of n = 5 enrolled patients is considered sufficient for statistical evaluations. The statistical analysis was performed using GraphPad Prism Software (v. 5.0). Mann–Whitney test was used for group comparisons. Fisher's test was used to compare VEGF or HIF-1α immunoreactive bands.

RESULTS

Submucosal Blood Vessel Assessment

As reported in Fig. 1*A*, the submucosal area occupied by vascular tissue in patients with MNGIE (12.6 ± 5.4 ratio) was 2.2-fold lower as compared with controls (28.4 ± 4.9 ratio; P = 0.002). Conversely, the number of blood vessels per mm^2 of submucosa was 2.1 times higher in patients with MNGIE (25.8 ± 16.0 number of vessels/mm^2) compared with controls (12.2 ± 4.8 number of vessels/mm^2; P = 0.019; (Fig. 1*B*). Compared with large and medium size blood vessels, those of small size were significantly more abundant in MNGIE (Fig. 1*C*). Compared with controls, there was a significant reduction in the percentage of large (Fig. 2, *A* and *B*) and medium (Fig. 2, *C* and *D*) size blood vessels (vessels >301 μm, 5.7% ± 4.9% vs. 15.9% ± 6.1% P = 0.0163; vessels 300–101 μm, 18.2% ± 8.0% vs. 41.1% ± 6.7% P = 0.0010) that corresponded to ~2.8- and 2.3-folds decrease, respectively, in patients with MNGIE. The percentage of small (100–51 μm) blood vessels did not change in MNGIE versus controls (24.3% ± 8.1% vs. 25.1% ± 7.6%) (Fig. 2, *E* and *F*), whereas the percentage of the very small vessels (<50 μm) was significantly higher 2.9-fold in patients with MNGIE (51.6% ± 18.3%) compared with controls (17.8% ± 7.7%; P = 0.001) (Fig. 2, *G* and *H*).

Fibrosis Assessment

The fibrosis index (Fig. 3*A*) was 1.7-fold higher in patients with MNGIE versus controls (1.7 ± 0.3 vs. 1 ± 0.2; P = 0.0043). The density of disorganized orcein-labeled elastic fibers was more abundant in the submucosal layer of patients with MNGIE compared with controls, where their detection was marginal or absent (Fig. 3, *B* and *C*). There was increased fibrosis as indicated by the abundant and disorganized Sirius red-labeled collagen/fast green in the submucosa (Fig. 3*E*) of patients

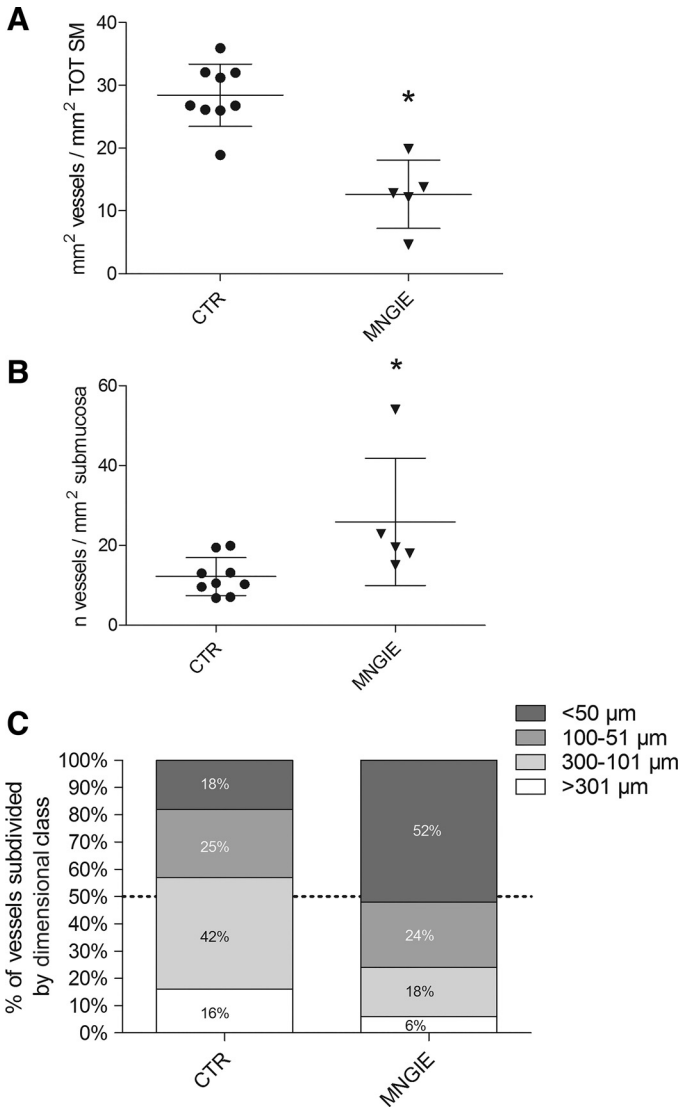

Figure 1. Measurement of vascular tissue of the submucosal layer. *A*: ratio of the area of submucosal layer occupied by vascular tissue expressed in mm^2 divided for the total area (mm^2) of submucosa in patients with MNGIE and controls (CTR) (*P = 0.0022). *B*: ratio between the number of total vessels counted in the submucosa divided for the total area (mm^2) of submucosa in patients with MNGIE and CTR (*P = 0.019). *C*: illustration of the percentage of each group of vessels separated on the basis of their diameter in the submucosa of patients with MNGIE and CTR. Note that in patients with MNGIE more than half of the vessels have the diameter < 50 μm. MNGIE, mitochondrial neurogastrointestinal encephalomyopathy.

with MNGIE compared with controls (Fig. 3*D*). There were also severe cellular abnormalities of the mucosal layer, and collagen fibers were clearly visualized throughout the lamina propria in patients with MNGIE. In addition, qualitative analysis of the structure of blood vessels revealed abnormalities including a very thin or even absent endothelium and a disorganized and collagen ("onion-like") enriched vascular wall in patients with MNGIE (Fig. 3*G*) compared with controls (Fig. 3*F*).

Longitudinal Muscle Layer Thickness

The thickness of the longitudinal muscle layer in patients with MNGIE was 4.6-fold lower as compared

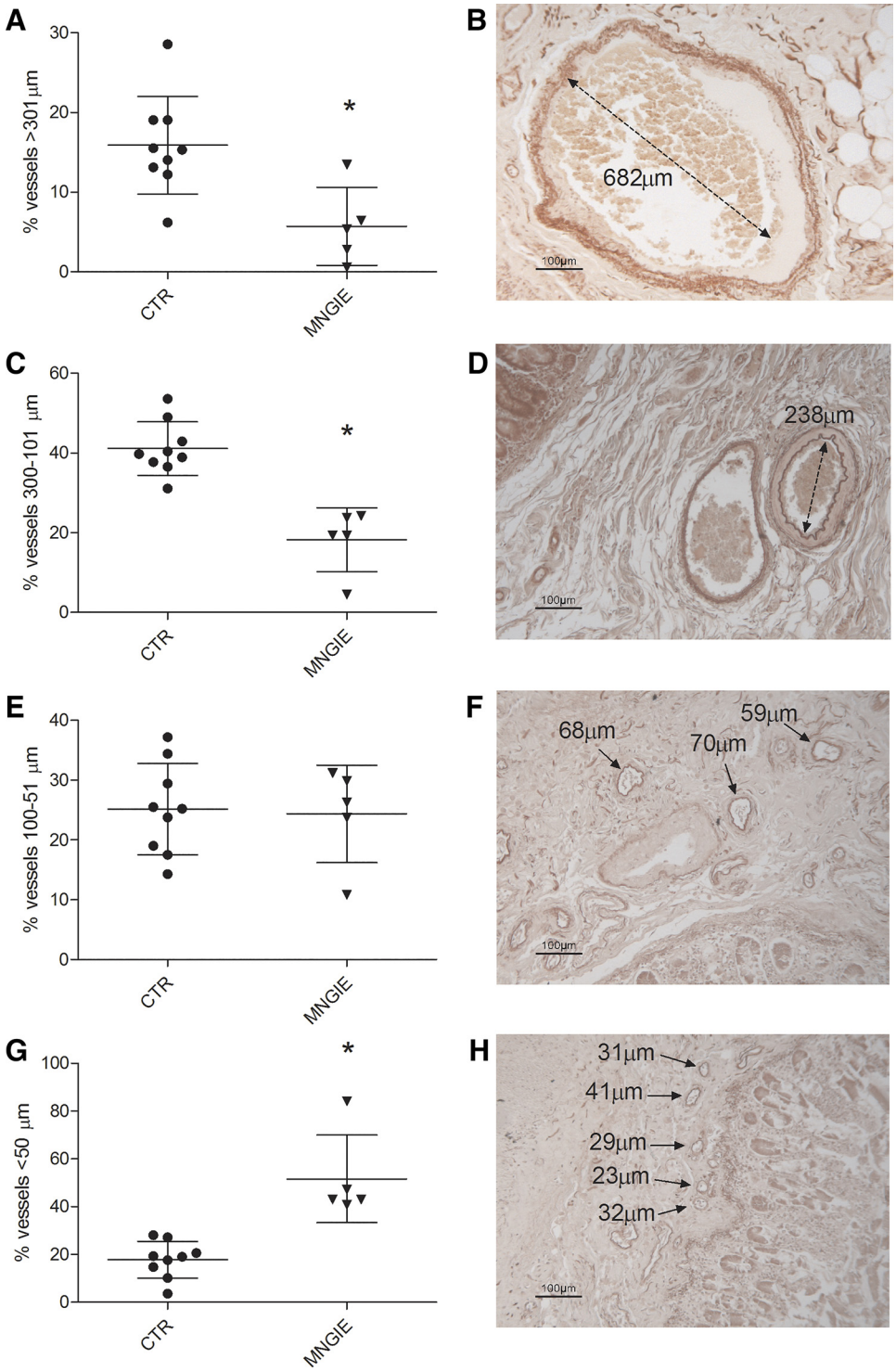

Figure 2. Analysis of different diameter submucosal vessels. *A*, *C*, *E*, and *G*: percentage of vessels of different diameter in each patient with MNGIE and CTR. *B*, *D*, *F*, and *H*: representative images of sections stained with orcein for each vessel size are shown in (magnification bar 100 µm). Specifically, graph reporting the percentage of large diameter vessels in CTR vs. patients with MNGIE (*P = 0.0163) (*A*) with a representative image of large vessel (> 301 µm) in *B*. Graph illustrating the percentage of medium diameter vessels in CTR vs. patients with MNGIE (*P = 0.001) (*C*) with a representative image of medium vessel (300–101 µm) in *D*. Graph showing the percentage of small vessels (P = ns) (*E*) with a representative image of small vessel (100–51 µm) in *F*. Graph showing the percentage of the smallest diameter vessels in both groups (*P = 0.001) (*G*) with a representative image of the smallest diameter vessel (<50 µm) in *H*. MNGIE, mitochondrial neurogastrointestinal encephalomyopathy.

with controls (307.8 ± 125.9 vs. 1,427.6 ± 980.1 µm; P = 0.0033) (Fig. 4, *A*–*C*). The muscle layer of patients with MNGIE showed a massive fibrosis particularly evident in the longitudinal layer compared with controls (Fig. 4, *D* and *E*) The fibrosis in the muscle wrapped around myenteric ganglia, thus generating a periganglionic cap.

Submucosal and Myenteric Neuron Cell Count and Interganglionic Distance Assessment

The quantitative analysis of neurons in the submucosal plexus showed no differences between patients with MNGIE and controls (3.4 ± 0.9 vs. 4.2 ± 1; P = 0.2389, respectively) (data not shown). The quantitative analysis of myenteric

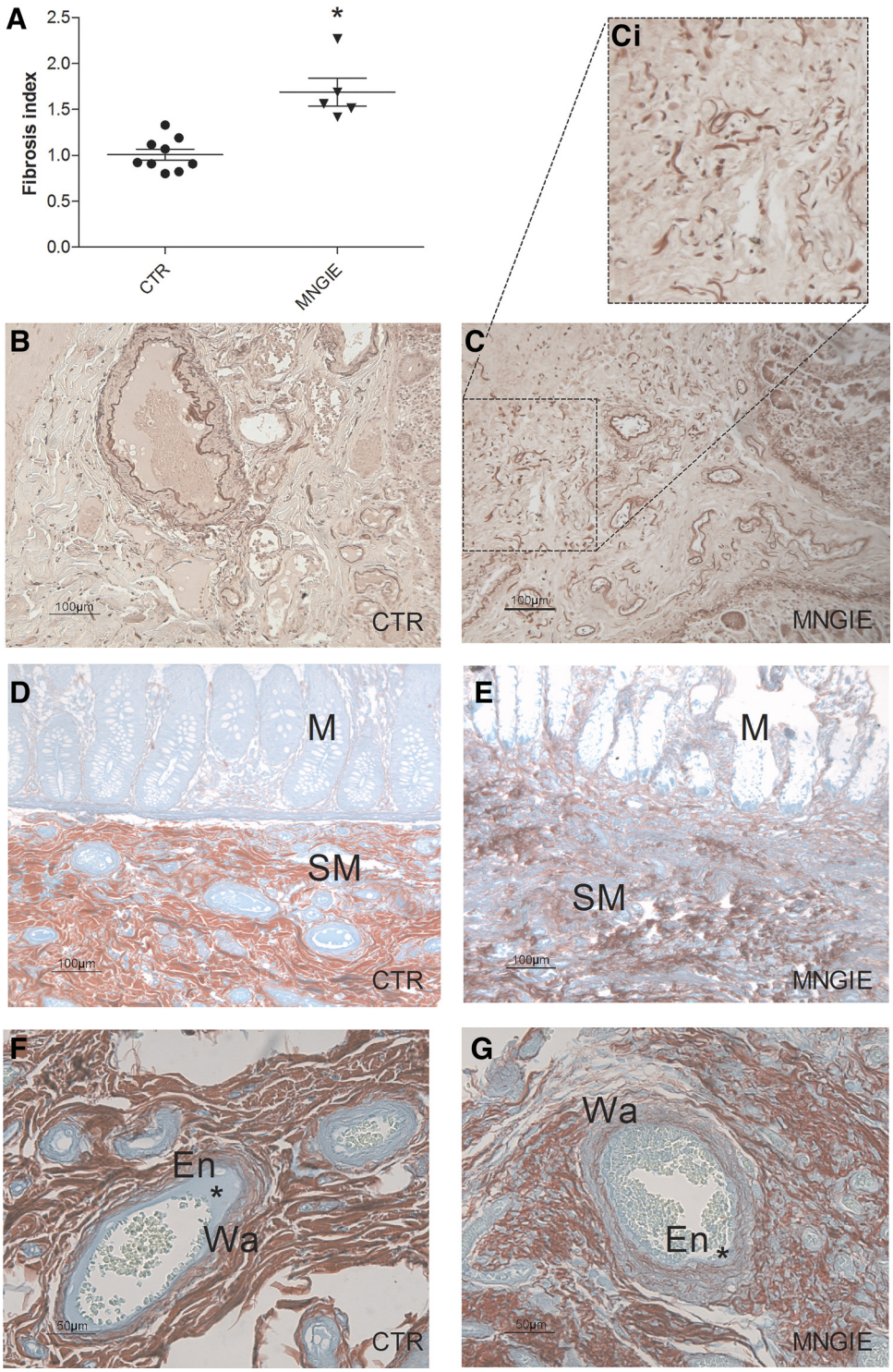

Figure 3. Fibrosis assessment on full-thickness biopsies of jejunal tissue. *A*: the graph shows the fibrosis index in the full-thickness jejunal biopsies that was significantly increased in patients with MNGIE vs. controls (*P = 0.0043). Sections of the jejunum submucosa in CTR (*B*) and patients with MNGIE (*C*); note the abundant and disorganized spread of elastic fibers in patients with MNGIE illustrated in *Ci* that is a high magnification of *C*, which are absent in controls. Images were obtained from orcein-stained tissue sections (magnification bar 100 μm). Sections from CTR (*D*) and patients with MNGIE (*E*), that were stained using Sirius red and fast green. Red color is the collagen distributed in mucosa (M) and submucosa (SM), whereas light green represents noncollagenous fibers (magnification bar 100 μm). Sections from CTR (*F*) and patients with MNGIE (*G*) are stained with Sirius red and fast green to label vessel structure, particularly vessel wall (Wa) and endothelium (En) in green and labeled with *. Calibration bar: 50 μm. CTR, control; MNGIE, mitochondrial neurogastrointestinal encephalomyopathy.

neurons is shown in Fig. 5, *A–C*. Patients with MNGIE showed a 4.6-fold lower number of neurons/ganglion compared with controls (11.2 ± 4.2 vs. 51.2 ± 9.6; P = 0.001). In line with this result, the interganglionic distance between adjacent myenteric ganglia was 2.2-fold higher (981.7 ± 266.4 μm) in patients with MNGIE compared with controls (447.7 ± 61.9 μm; P = 0.001) (Fig. 5, *D–F*).

HIF-1α and VEGF Tissue Distribution and WB Detection

In contrast to controls (Fig. 6, *A–C*), jejunum tissue sections of patients with MNGIE (Fig. 6, *D–G*) showed intense HIF-1α immunoreactivity detected in both longitudinal (Fig. 6*D*) and circular (Fig. 6*F*) muscle layers and in some myenteric ganglia (Fig. 6*E*). A progressive increase of HIF-1α

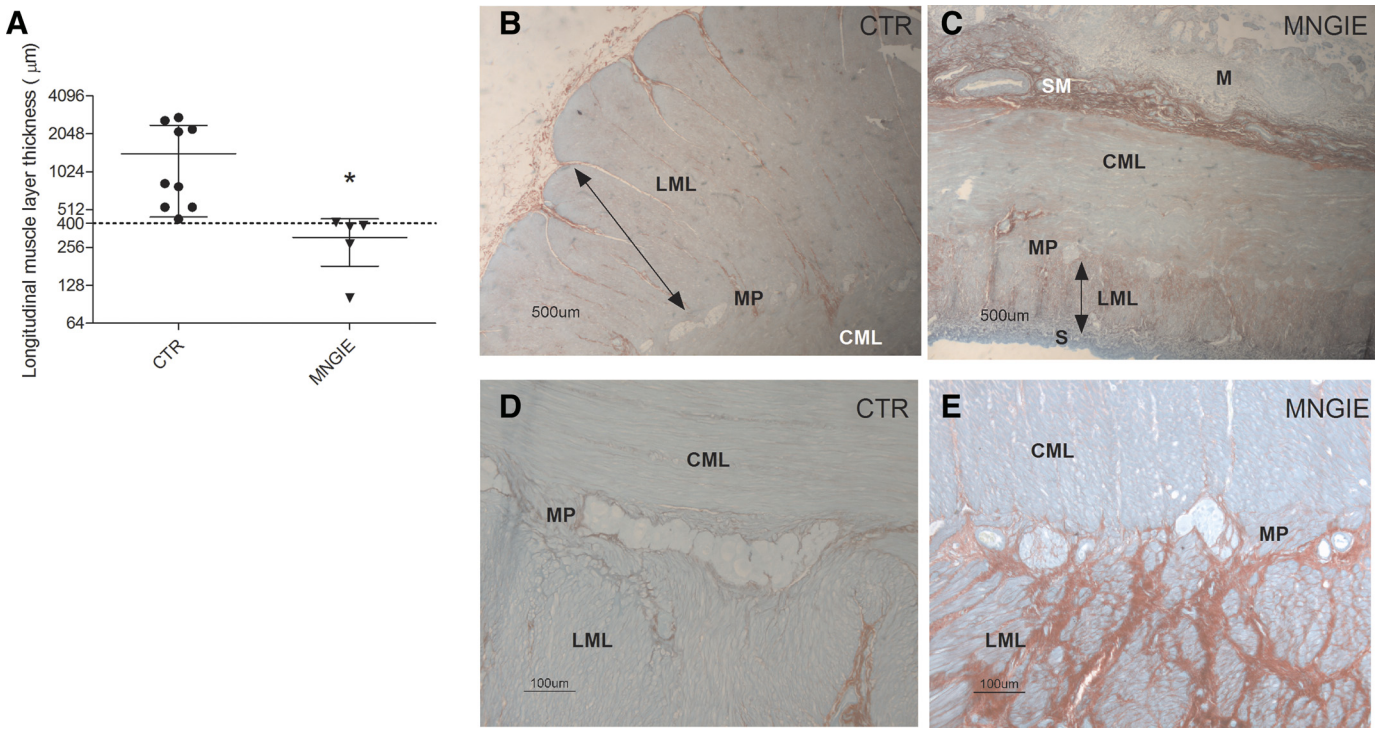

Figure 4. Longitudinal muscle quantitative and qualitative assessment. *A*: graph showing the difference in thickness of the external longitudinal muscle layer in controls (CTR) and patients with MNGIE (*P = 0.0033). Tissue sections from CTR (*B*) and patients with MNGIE (*C*), which are stained with Sirius red and fast green. The black double arrows in *B* and *C* indicate the thickness of the external longitudinal muscle layer (LML). Magnification bar: 500 μm. Section stained with Sirius red and fast green in CTR (*D*) and patients with MNGIE (*E*). In *E*, the majority of muscle cells (light green) of the LML are substituted by collagen fibers (red). The MP in patients with MNGIE is deeply enveloped in collagen. Note the increased collagen expression visible in the CML (magnification bar: 100 μm). CML, inner circular muscle layer; M, mucosa; MNGIE, mitochondrial neurogastrointestinal encephalomyopathy; MP, myenteric plexus; S, serosa; SM, submucosa.

immunoreactivity was appreciated from the innermost to the outermost aspects of the muscle layer (Fig. 6*G*). Western blot analysis confirmed that HIF-1α expression was detected in MNGIE but it was under the detection limit in control jejunal extracts ($P < 0.001$) (Fig. 6, *H* and *I*).

In contrast to controls (Fig. 7, *A* and *C*), where only a few VEGF-positive vessels were detectable in the jejunal submucosa, patients with MNGIE displayed an abundant number of very small VEGF-positive vessels (Fig. 7, *B* and *D*). As highlighted in Fig. 7*D*, some of these VEGF-positive vessels showed damages, such as an apparently broken wall. In contrast to controls, Western blot analysis of VEGF yielded a four time more abundant expression in patients with MNGIE versus controls (1.6 ± 0.7 vs. 0.4 ± 0.2) in full-thickness tissue protein extracts ($P < 0.05$) (Fig. 7, *E* and *F*).

As previously indicated, WB quantification was possible only in 2 patients with MNGIE. Despite the very low number of cases, the difference is statistically significant. However, these data confirmed the immunohistochemical analysis and the antibody specificity performed in all cases.

DISCUSSION

This study was designed to perform a thorough morphometric evaluation of the blood vessels, fibrosis index, and enteric neuron density in jejunal full-thickness biopsies of patients with MNGIE compared with controls and establish whether hypoxic mechanisms may underlie the occurrence and persistence of GI symptoms and complications in patients with MNGIE.

In the GI tract, blood vessels in the submucous layer predominantly originate from the trunks of vasa recta, their collaterals or mutual anastomosis. A negligible vascular contribution to GI muscular layers derives from the subserous plexus (18). Our analysis showed that 57% of the vasculature in the submucosa of the jejunum of patients with MNGIE had a diameter lower than 100 μm and in this subset 52% of blood vessels had a diameter lower than 50 μm. Only 24% of the total vessels had a diameter >300 μm. In contrast, in control submucosa, 58% of vessels had a diameter >300 μm and only 18% had a diameter < 50 μm. The striking difference in blood vessel sizes explains the marked decrease in the total area of vascular tissue observed in the submucosal layer of patients with MNGIE versus controls. Taken together, our data support the existence of significant vascular abnormalities in the jejunum of patients with MNGIE that are likely related to the absence of TP activity, which most probably impacts angiogenesis and vascular maintenance.

Angiogenesis is a finely tuned process involving several factors that cooperate in a coordinated manner. Among the factors playing a role in blood vessel formation, vascular VEGF and TP are known to exert a regulatory effect on endothelial cell migration, which is required to generate the prelumen of vessels (19). Specifically, TP is thought to act via a secondary mediator, named dRP, a pentose monosaccharide with a phosphate group bound to carbon 1, that originates

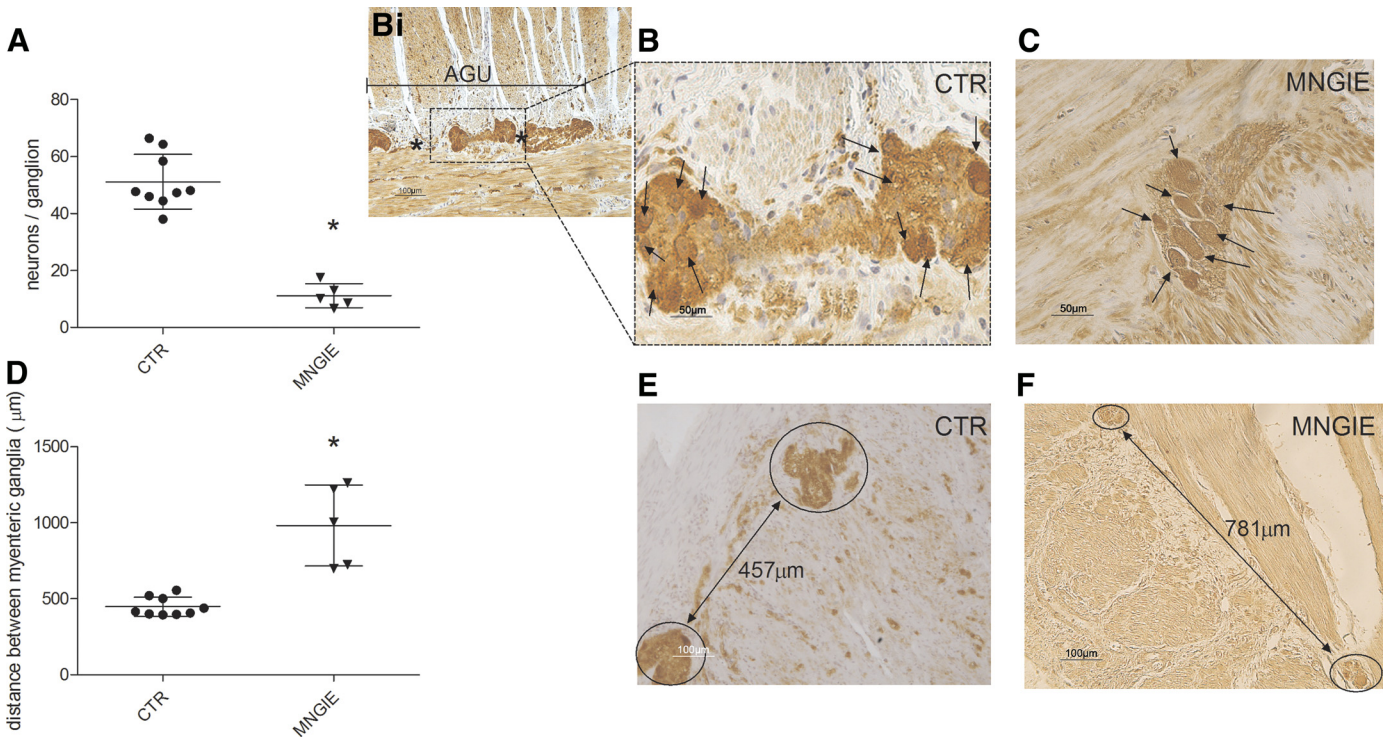

Figure 5. Myenteric plexus quantitative analysis. *A*: graph shows the number of neuronal cell bodies calculated per ganglion for each patient that was significantly decreased in patients with MNGIE vs. CTR (*P = 0.001). Neuron-specific enolase (NSE) immunoreactivity in tissue sections from CTR (*B*) and patients with MNGIE (*C*). The black arrows point to neuronal cell bodies (magnification bar: 50 µm). *C* from a biopsy of patients with MNGIE shows the entire ganglion, whereas *B* shows a portion of a ganglion from a control. *B* is a high magnification of the *inset* in the dotted area in *Bi*, which is a low-magnification image. In *Bi,* the two * indicate a distance lower than 300 µm, which is the cut-off we have previously established to define the arbitrary ganglionic unit in thin sections (17), thus NSE immunoreactive neurons within this area belong to the same arbitrary ganglionic unit (AGU) (17). *D*: graph shows the interganglionic distance calculated on neighboring ganglia for each patient, which is much higher in patients with MNGIE compared with CTR (*P = 0.001). The distance between adjacent ganglia visualized with NSE immunostaining in CTR (*E*) and patients with MNGIE (*F*). Black arrows indicate the distance between two ganglia in CTR (*E*) and patients with MNGIE (*F*). CTR, control; MNGIE, mitochondrial neurogastrointestinal encephalomyopathy.

during the TP-mediated conversion of the nucleosides (thymidine and deoxy-uridine) into the corresponding nucleotides (thymine and uracil) (12). The local release of dRP evokes a chemotactic effect on endothelial cells, which migrate from neighboring regions and initiate blood vessel formation (20–22). The genetically driven defective TP in patients with MNGIE does not allow the local release of dRP, likely leading to vascular abnormalities. As TYMP and VEGF expression is known to be mutually influenced (23), the lack of TP can be compensated by VEGF as supported by our data showing a significant number of small size VEGF-positive vessels, a finding suggestive of an active neo-angiogenesis, in the jejunum of patients with MNGIE. Furthermore, other studies showed that an increased VEGF expression results in excessively leaky (12), permeable (24), and fragile vessels (25). Indeed, though these features require further investigation, in our study, we have identified VEGF-positive damaged vascular walls in MNGIE specimens but not in controls. One of the most serious clinical consequences that patients with MNGIE may experience is GI bleeding, a possible life-threatening complication of the disease (10). The emerging evidence supporting the hypothesis of a fragile and permeable microvascular system is further reinforced by reported cases such as that of a 25-yr-old female with MNGIE who received AHSCT and had repeated episodes of severe anemia due to heavy GI bleeding 3 yr after transplantation. GI endoscopy biopsies demonstrated marked vascular abnormalities (26), as important risk factors underlying GI complications, sometimes with fatal outcome.

In our study, we demonstrated a shift of the microvascular pattern showing an increase of the number and area occupied by small size compared with medium and large size vessels in the jejunal submucosa of patients with MNGIE versus controls. It is reasonable to hypothesize that the prevalence of small size vessels causes inadequate blood flow resulting in hypoxia responsible of tissue changes such as pronounced fibrosis, involving tissues underneath the submucosa. In view of this hypothesis, we quantitatively assessed the tissue-specific fibrosis index, the distribution of collagen in the different GI layers and HIF-1α protein expression and localization.

In addition to previously reported molecular and morphological data (14, 27), the increased fibrosis index in the longitudinal muscle and myenteric plexuses along with the increased expression of HIF-1α in the muscular layer and myenteric neurons, corroborate the hypothesis of hypoxia as a mechanism affecting the muscular and neuronal integrity in the small intestine of patients with MNGIE.

A tight relationship between vascular endothelial cells proliferation and collagen has been documented by several studies (28–34). The major constituent of the vessel wall is the extracellular matrix, which is composed by 50% of

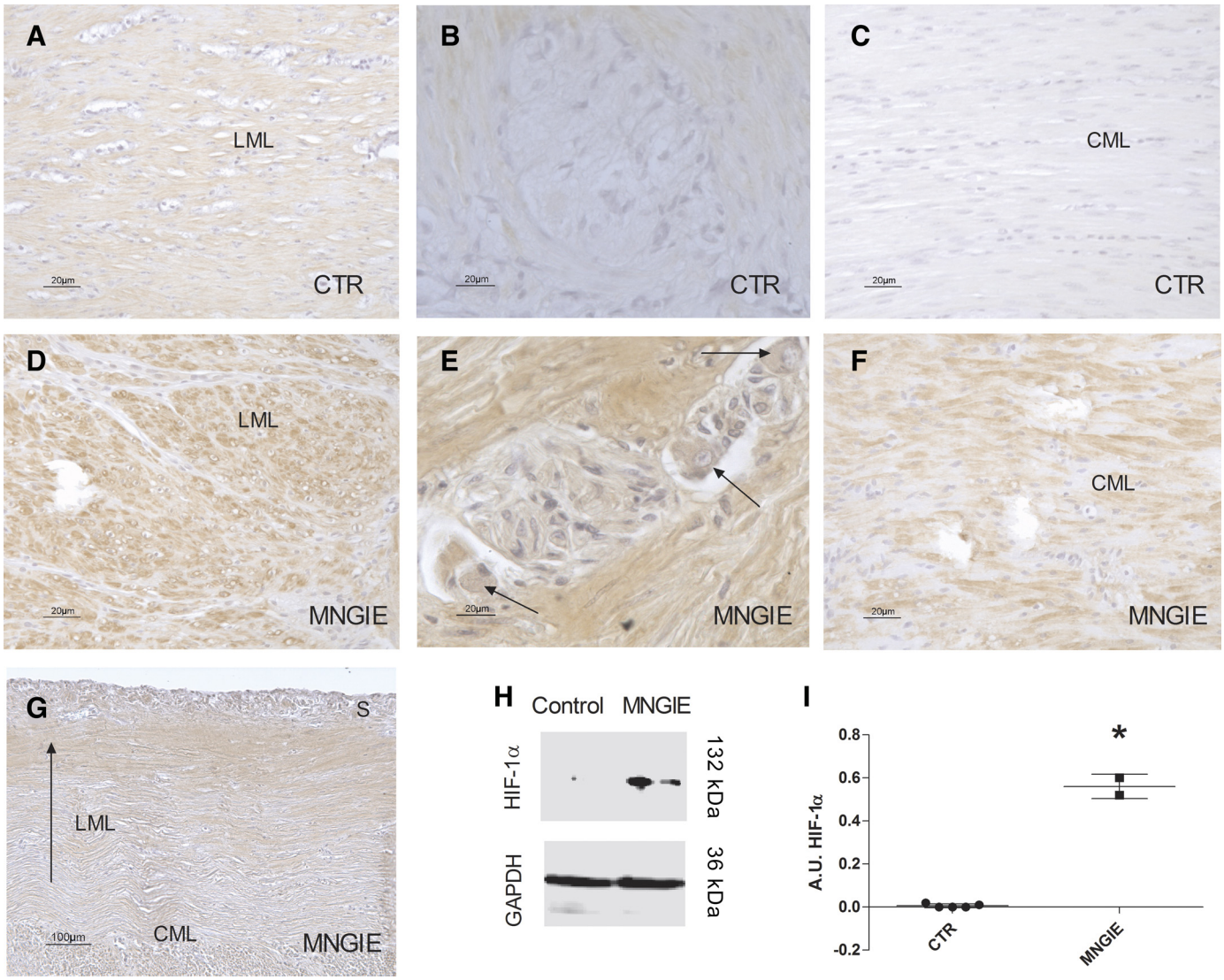

Figure 6. HIF-1α protein localization and expression. Tissue sections from CTR (*A*–*C*) and patients with MNGIE (*D*–*F*) stained with HIF-1α protein antibodies. Note the intense immunostaining in the longitudinal muscle layer (LML) (*D*), myenteric ganglia (*E*), and circular muscle layer (CML) (*F*) of patients with MNGIE compared with the lack of staining in CTR (*A*–*C*). Black arrows in *E* point to HIF-1α-positive neurons (magnification bar: 20 μm). *G*: the increase gradient of immunostaining intensity in the LML of tissue sections of patients with MNGIE from the circular muscle layer (CML, *bottom*) (lowest intensity) to the serosa (S, *top*) (highest intensity) (100 μm scale bar). *H* and *I*: the increase in HIF-1α jejunal protein expression in Western blotting from patients with MNGIE and CTR. HIF-1α jejunal protein expression was normalized vs. GAPDH (reference protein) and expressed in densitometry arbitrary unit (AU), $*P < 0.001$. CTR, control; HIF-1α, hypoxia-inducible-factor-1α; MNGIE, mitochondrial neurogastrointestinal encephalomyopathy.

collagen and elastin. The synthesis and metabolism of these matrix proteins are finely regulated to preserve the blood vessel structure and function. Vascular wall matrix remodeling alters vessels that may become narrow, stiff, and easy to break or undergo aneurismal changes. Blood vessels of patients with MNGIE show a very thin, virtually absent, endothelium coupled with an excessive fibrosis due to an increased deposition of collagen that significantly alters the vascular wall structure. These abnormalities may persist even in patients with MNGIE receiving TP replacement and can progress toward complications, such as GI bleeding (10). It can be speculated that only a local release of TP may be effective to rescue a normal vascularization. In addition, mutations, deficiencies or different composition of collagen directly or indirectly affect vasculature structure that could complicate with bleeding (34). The vascular alterations with a prominent change of vascular phenotype, that is, from large to small size blood vessels, detected in the GI tract of patients with MNGIE may be the cause of irreversible damage to the GI tract. In addition, the natural history of MNGIE implies progressive metabolic tissue impairment due to mtDNA depletion, secondary to toxic thymidine levels in circulating blood, and we previously documented that this is reflected by defective oxidative phosphorylation in brain vessels (9).

In addition to vasculature, the hypoxia/fibrosis-related changes affect the myenteric plexus of the jejunum of patients with MNGIE. Although neurons appeared

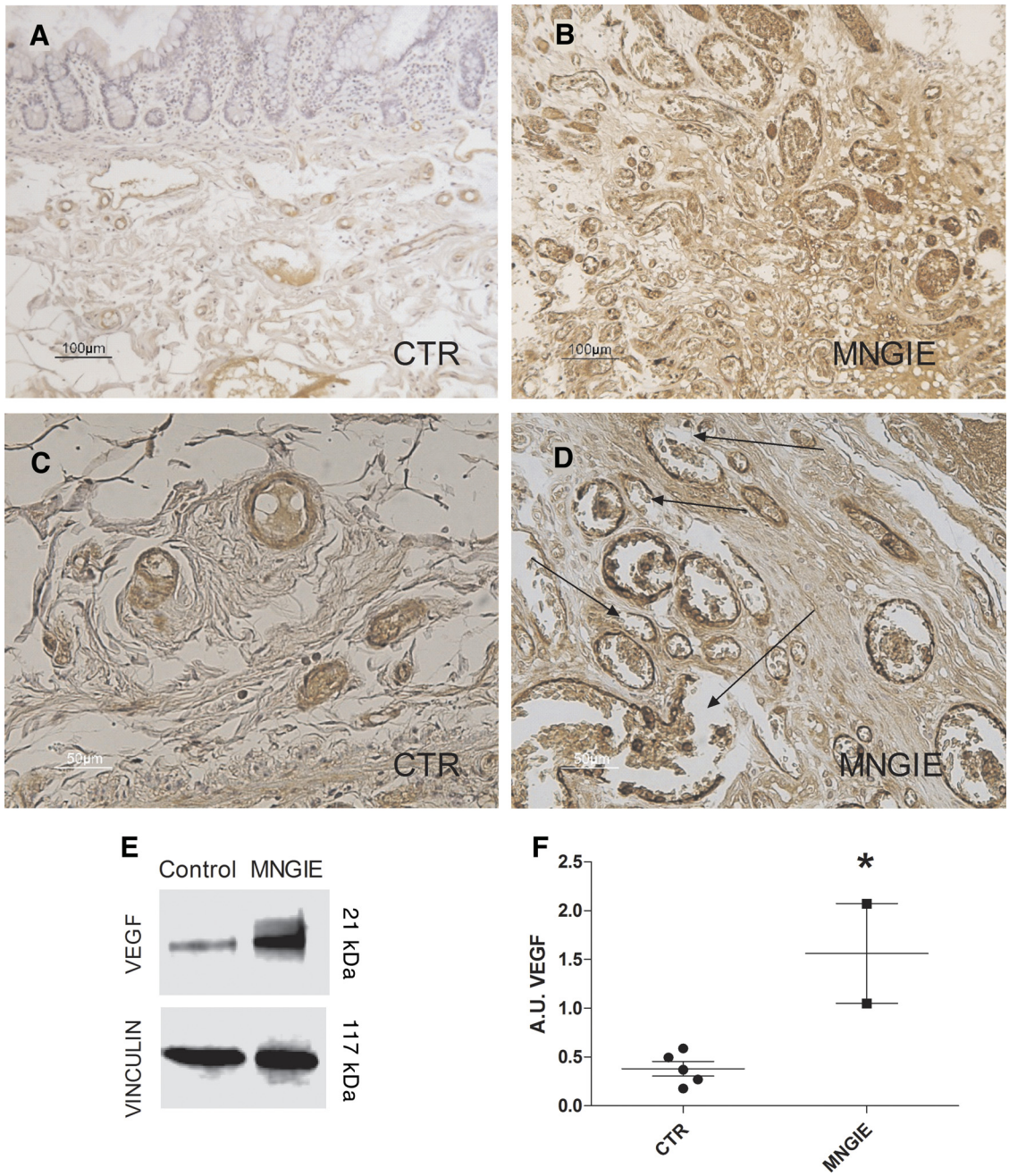

Figure 7. VEGF protein localization and expression. VEGF immunoreactivity in submucosal vessels in tissue sections from control (CTR) (*A*), and patients with MNGIE (*B*) (100 μm scale bar). High magnification images of submucosal vessels expressing VEGF immunoreactivity in tissue sections from CTR (*C*) and patients with MNGIE (*D*) (50 μm scale bar). Black arrows in *D* point to vessels with a fragmented wall. *E*: VEGF immunoreactive bands in Western blotting from CTR and patients with MNGIE jejunal tissues. *F*: quantification of VEGF jejunal protein expression normalized vs. VINCULIN (reference protein) and expressed in densitometry arbitrary unit (AU), $*P < 0.05$. MNGIE, mitochondrial neurogastrointestinal encephalomyopathy; VEGF, vascular endothelial cell growth factor.

qualitatively and morphologically normal at a histopathological analysis, we identified two aspects indicative of neuropathology (14, 17), that is, an increased interganglionic distance between adjacent ganglia and a drastic reduction in the number of myenteric, but not submucosal, neurons per ganglion. In addition, some myenteric neurons in patients with MNGIE are HIF-1α positive, indicating hypoxic conditions in the plexus. These neuronal abnormalities observed in patients with MNGIE may be ascribed to the low oxygen environment due to the altered vasculature and the collagen cap surrounding ganglia, probably secondary to the fibrosis progression. The finding that submucosal neurons in patients with MNGIE do not appear altered supports the possibility that the reduced blood flow may reach the submucosa in the short-range, but not the deeper gut layer (i.e., myenteric plexus and longitudinal muscle layer) because of major microvascular abnormalities.

In conclusion, our study showed that the GI vasculature architecture is altered in the jejunal submucosa of patients with MNGIE as indicated by the decrease in the area of vascular tissue due to the prevalence of vessels with a low diameter (<50 μm) compared with those with medium/large size (between 100 μm and 300 μm). These changes were associated with HIF-1α-mediated hypoxia and the consequent severe tissue fibrosis (mainly detectable in the longitudinal muscle layer) coupled with a lower number of myenteric neurons and an increase of the myenteric interganglionic distance. The lack of TP and the HIF-1α upregulation may induce VEGF-mediated angiogenesis with abnormal neovascularization. A possible limitation of our study is related to the low number of samples analyzed. However, because MNGIE is an ultrarare disease and the data are consistent and reproducible, $n = 5$ has been considered a sufficient number of cases to provide statistically significant results. Thus, MNGIE may be thought as a condition with an underling angiopathy. Overall, our results suggest that the vascular tissue abnormalities, which may be not corrected by AHSCT or LT, are responsible for the permanent GI alterations occurring in MNGIE, paving the way to evaluate organ revascularization strategies after TP replacement.

DATA AVAILABILITY

All data which have been generated, analyzed, and discussed in this study have been included in this published article. The data sets obtained during the current study are available from the corresponding author on reasonable request.

GRANTS

C. Sternini was supported by the Imaging and Stem Cell Biology Core, National Institute of Diabetes and Digestive and Kidney Diseases Grant P30 DK-41301. V. Carelli is supported by the Ricerca Corrente funding from the Italian Ministry of Health. R. De Giorgio is supported by Fondi Ateneo per la Ricerca (FAR) and Fondi Incentivazione alla Ricerca (FIR) Research Funds from the University of Ferrara, Ferrara, Italy.

DISCLOSURES

No conflicts of interest, financial or otherwise, are declared by the authors.

AUTHOR CONTRIBUTIONS

E.B., G.C., V.S., C.S., R.R., V.C., and R.D.G. conceived and designed research; E.B., R.D., and C.M. performed experiments; E.B., R.D., M.L.T., R.C., C.G., A.A., and G.C. analyzed data; E.B., R.D., M.L.T., R.C., C.G., A.A., C.M., P.C., V.T., G.C., V.R., C.G., A.D., G.C., M.T.D., V.S., C.S., L.P., R.R., V.C., and R.D.G. interpreted results of experiments; E.B., M.T.D., C.S., V.C., and R.D.G. prepared figures; E.B., C.S., R.R., V.C., and R.D.G. drafted manuscript; E.B., R.C., A.A., C.M., P.C., G.C., V.R., C.G., A.D., G.C., V.S., C.S., R.R., V.C., and R.D.G. edited and revised manuscript; E.B., R.D., M.L.T., R.C., C.G., A.A., C.M., P.C., V.T., G.C., V.R., C.G., A.D., G.C., M.T.D., V.S., C.S., L.P., R.R., V.C., and R.D.G. approved final version of manuscript.

REFERENCES

1. **Hirano M**, **Carelli V**, **De Giorgio R**, **Pironi L**, **Accarino A**, **Cenacchi G, et al.** Mitochondrial neurogastrointestinal encephalomyopathy (MNGIE): Position paper on diagnosis, prognosis, and treatment by the MNGIE International Network. *J Inherit Metab Dis* 1–12, 2020. doi:10.1002/jimd.12300.
2. **Hirano M**, **Marti R**, **Spinazzola A**, **Nishino I**, **Nishigaki Y.** Thymidine phosphorylase deficiency causes MNGIE: an autosomal recessive mitochondrial disorder. *Nucleosides Nucleotides Nucleic Acids* 23: 1217–1225, 2004. doi:10.1081/NCN-200027485.
3. **Hirano M**, **Silvestri G**, **Blake DM**, **Lombes A**, **Minetti C**, **Bonilla E**, **Hays AP**, **Lovelace RE**, **Butler I**, **Bertorini TE.** and Mitochondrial neurogastrointestinal encephalomyopathy (MNGIE): clinical, biochemical, and genetic features of an autosomal recessive mitochondrial disorder. *Neurology* 44: 721–727, 1994. doi:10.1212/wnl.44.4.721.
4. **De Giorgio R**, **Pironi L**, **Rinaldi R**, **Boschetti E**, **Caporali L**, **Capristo M**, **Casali C**, **Cenacchi G**, **Contin M**, **D'Angelo R**, **D'Errico A**, **Gramegna LL**, **Lodi R**, **Maresca A**, **Mohamed S**, **Morelli MC**, **Papa V**, **Tonon C**, **Tugnoli V**, **Carelli V**, **D'Alessandro R**, **Pinna AD.** Liver transplantation for mitochondrial neurogastrointestinal encephalomyopathy. *Ann Neurol* 80: 448–455, 2016. doi:10.1002/ana.24724.
5. **Halter JP**, **Michael W**, **Schupbach M**, **Mandel H**, **Casali C**, **Orchard K**, et al**.** Allogeneic haematopoietic stem cell transplantation for mitochondrial neurogastrointestinal encephalomyopathy. *Brain* 138: 2847–2858, 2015. doi:10.1093/brain/awv226.
6. **Filosto M**, **Scarpelli M**, **Tonin P**, **Lucchini G**, **Pavan F**, **Santus F**, **Parini R**, **Donati MA**, **Cotelli MS**, **Vielmi V**, **Todeschini A**, **Canonico F**, **Tomelleri G**, **Padovani A**, **Rovelli A.** Course and management of allogeneic stem cell transplantation in patients with mitochondrial neurogastrointestinal encephalomyopathy. *J Neurol* 259: 2699–2706, 2012. doi:10.1007/s00415-012-6572-9.
7. **Gramegna LL**, **Pisano A**, **Testa C**, **Manners DN**, **D'Angelo R**, **Boschetti E**, **Giancola F**, **Pironi L**, **Caporali L**, **Capristo M**, **Valentino ML**, **Plazzi G**, **Casali C**, **Dotti MT**, **Cenacchi G**, **Hirano M**, **Giordano C**, **Parchi P**, **Rinaldi R**, **De Giorgio R**, **Lodi R**, **Carelli V**, **Tonon C.** Cerebral mitochondrial microangiopathy leads to leukoencephalopathy in mitochondrial neurogastrointestinal encephalopathy. *AJNR Am J Neuroradiol* 39: 427–434, 2018. doi:10.3174/ajnr.A5507.
8. **Boschetti E**, **D'Alessandro R**, **Bianco F**, **Carelli V**, **Cenacchi G**, **Pinna AD**, **Del Gaudio M**, **Rinaldi R**, **Stanghellini V**, **Pironi L**, **Rhoden K**, **Tugnoli V**, **Casali C**, **De Giorgio R.** Liver as a source for thymidine phosphorylase replacement in mitochondrial neurogastrointestinal encephalomyopathy. *PLoS One* 9: e96692, 2014. doi:10.1371/journal.pone.0096692.
9. **D'Angelo R**, **Rinaldi R**, **Carelli V**, **Boschetti E**, **Caporali L**, **Capristo M**, **Casali C**, **Cenacchi G**, **Gramegna LL**, **Lodi R**, **Pinna AD**, **Pironi L**, **Stanzani M**, **Tonon C**, **D'Alessandro R**, **De Giorgio R.** ITA-MNGIE: an Italian regional and national survey for mitochondrial neuro-gastro-intestinal encephalomyopathy. *Neurol Sci* 37: 1149–1151, 2016. doi:10.1007/s10072-016-2552-7.
10. **D'Angelo R**, **Boschetti E**, **Amore G**, **Costa R**, **Pugliese A**, **Caporali L**, **Gramegna LL**, **Papa V**, **Vizioli L**, **Capristo M**, **Contin M**, **Mohamed S**, **Cenacchi G**, **Lodi R**, **Morelli MC**, **Fasano L**, **Pisani L**, **Cescon M**, **Tonon C**, **Pinna AD**, **Dotti MT**, **Sicurelli F**, **Scarpelli M**, **Filosto M**, **Casali C**, **Pironi L**, **Carelli V**, **Giorgio RD**, **Rinaldi R.** Liver transplantation in mitochondrial neurogastrointestinal encephalomyopathy (MNGIE): clinical long-term follow-up and pathogenic implications. *J Neurol* 267: 3702–3710, 2020. doi:10.1007/s00415-020-10051-x.
11. **Papetti M**, **Herman IM.** Mechanisms of normal and tumor-derived angiogenesis. *Am J Physiol Cell Physiol* 282: C947–C970, 2002. doi:10.1152/ajpcell.00389.2001.
12. **Yancopoulos GD**, **Davis S**, **Gale NW**, **Rudge JS**, **Wiegand SJ**, **Holash J.** Vascular-specific growth factors and blood vessel formation. *Nature* 407: 242–248, 2000. doi:10.1038/35025215.
13. **Dikici S**, **Aldemir Dikici B**, **Bhaloo SI**, **Balcells M**, **Edelman ER**, **MacNeil S**, **Reilly GC**, **Sherborne C**, **Claeyssens F.** Assessment of the angiogenic potential of 2-deoxy-D-ribose using a novel in vitro 3D dynamic model in comparison with established in vitro assays. *Front Bioeng Biotechnol* 7: 451, 2019. doi:10.3389/fbioe.2019.00451.
14. **Giordano C**, **Sebastiani M**, **De Giorgio R**, **Travaglini C**, **Tancredi A**, **Valentino ML**, **Bellan M**, **Cossarizza A**, **Hirano M**, **d'Amati G**, **Carelli V.** Gastrointestinal dysmotility in mitochondrial neurogastrointestinal

encephalomyopathy is caused by mitochondrial DNA depletion. *Am J Pathol* 173: 1120–1128, 2008. doi:10.2353/ajpath.2008.080252.

15. **Giordano C**, **Sebastiani M**, **Plazzi G**, **Travaglini C**, **Sale P**, **Pinti M**, **Tancredi A**, **Liguori R**, **Montagna P**, **Bellan M**, **Valentino ML**, **Cossarizza A**, **Hirano M**, **d'Amati G**, **Carelli V.** Mitochondrial neurogastrointestinal encephalomyopathy: evidence of mitochondrial DNA depletion in the small intestine. *Gastroenterology* 130: 893–901, 2006. doi:10.1053/j.gastro.2006.01.004.
16. **Knowles CH**, **De Giorgio R**, **Kapur RP**, **Bruder E**, **Farrugia G**, **Geboes K**, **Gershon MD**, **Hutson J**, **Lindberg G**, **Martin JE**, **Meier-Ruge WA**, **Milla PJ**, **Smith VV**, **Vandervinden JM**, **Veress B**, **Wedel T.** Gastrointestinal neuromuscular pathology: guidelines for histological techniques and reporting on behalf of the Gastro 2009 International Working Group. *Acta Neuropathol* 118: 271–301, 2009. doi:10.1007/s00401-009-0527-y.
17. **Boschetti E**, **Malagelada C**, **Accarino A**, **Malagelada JR**, **Cogliandro RF**, **Gori A**, **Bonora E**, **Giancola F**, **Bianco F**, **Tugnoli V**, **Clavenzani P**, **Azpiroz F**, **Stanghellini V**, **Sternini C**, **De Giorgio R.** Enteric neuron density correlates with clinical features of severe gut dysmotility. *Am J Physiol Gastrointest Liver Physiol* 317: G793–G801, 2019. doi:10.1152/ajpgi.00199.2019.
18. **Kachlik D**, **Baca V**, **Stingl J.** The spatial arrangement of the human large intestinal wall blood circulation. *J Anat* 216: 335–343, 2010. doi:10.1111/j.1469-7580.2009.01199.x.
19. **Ferrara N.** VEGF-A: a critical regulator of blood vessel growth. *Eur Cytokine Netw* 20: 158–163, 2009. doi:10.1684/ecn.2009.0170.
20. **Azam M**, **Dikici S**, **Roman S**, **Mehmood A**, **Chaudhry AA**, **I UR**, **MacNeil S**, **Yar M.** Addition of 2-deoxy-d-ribose to clinically used alginate dressings stimulates angiogenesis and accelerates wound healing in diabetic rats. *J Biomater Appl* 34: 463–475, 2019. doi:10.1177/0885328219859991.
21. **Haraguchi M**, **Miyadera K**, **Uemura K**, **Sumizawa T**, **Furukawa T**, **Yamada K**, **Akiyama S**, **Yamada Y.** Angiogenic activity of enzymes. *Nature* 368: 198, 1994. doi:10.1038/368198a0.
22. **Matsushita S**, **Nitanda T**, **Furukawa T**, **Sumizawa T**, **Tani A**, **Nishimoto K**, **Akiba S**, **Miyadera K**, **Fukushima M**, **Yamada Y**, **Yoshida H**, **Kanzaki T**, **Akiyama S.** The effect of a thymidine phosphorylase inhibitor on angiogenesis and apoptosis in tumors. *Cancer Res* 59: 1911–1916, 1999.
23. **Chapouly C**, **Argaw AT**, **Horng S**, **Castro K**, **Zhang J**, **Asp L**, **Loo H**, **Laitman BM**, **Mariani JN**, **Farber RS**, **Zaslavsky E**, **Nudelman G**, **Raine CS**, **John GR.** Astrocytic TYMP and VEGFA drive blood-brain barrier opening in inflammatory central nervous system lesions. *Brain* 138: 1548–1567, 2015. doi:10.1093/brain/awv077.
24. **Cao R**, **Eriksson A**, **Kubo H**, **Alitalo K**, **Cao Y**, **Thyberg J.** Comparative evaluation of FGF-2-, VEGF-A-, and VEGF-C-induced angiogenesis, lymphangiogenesis, vascular fenestrations, and permeability. *Circ Res* 94: 664–670, 2004. doi:10.1161/01.RES.0000118600.91698.BB.
25. **Cheng SY**, **Nagane M**, **Huang HS**, **Cavenee WK.** Intracerebral tumor-associated hemorrhage caused by overexpression of the vascular endothelial growth factor isoforms VEGF121 and VEGF165 but not VEGF189. *Proc Natl Acad Sci USA* 94: 12081–12087, 1997. doi:10.1073/pnas.94.22.12081.
26. **Sicurelli F**, **Carluccio MA**, **Toraldo F**, **Tozzi M**, **Bucalossi A**, **Lenoci M**, **Jacomelli G**, **Micheli V**, **Cardaioli E**, **Mondelli M**, **Federico A**, **Marotta G**, **Dotti MT.** Clinical and biochemical improvement following HSCT in a patient with MNGIE: 1-year follow-up. *J Neurol* 259: 1985–1987, 2012. doi:10.1007/s00415-012-6500-z.
27. **Perez-Atayde AR.** Diagnosis of mitochondrial neurogastrointestinal encephalopathy disease in gastrointestinal biopsies. *Hum Pathol* 44: 1440–1446, 2013. doi:10.1016/j.humpath.2012.12.005.
28. **De Paepe A**, **Malfait F.** Bleeding and bruising in patients with Ehlers-Danlos syndrome and other collagen vascular disorders. *Br J Haematol* 127: 491–500, 2004. doi:10.1111/j.1365-2141.2004.05220.x.
29. **Deguchi JO**, **Huang H**, **Libby P**, **Aikawa E**, **Whittaker P**, **Sylvan J**, **Lee RT**, **Aikawa M.** Genetically engineered resistance for MMP collagenases promotes abdominal aortic aneurysm formation in mice infused with angiotensin II. *Lab Invest* 89: 315–326, 2009. doi:10.1038/labinvest.2008.167.
30. **Kuivaniemi H**, **Tromp G**, **Prockop DJ.** Mutations in fibrillar collagens (types I, II, III, and XI), fibril-associated collagen (type IX), and network-forming collagen (type X) cause a spectrum of diseases of bone, cartilage, and blood vessels. *Hum Mutat* 9: 300–315, 1997. doi:10.1002/(SICI)1098-1004(1997)9:4<300::AID-HUMU2>3.0.CO;2-9.
31. **Lohler J**, **Timpl R**, **Jaenisch R.** Embryonic lethal mutation in mouse collagen I gene causes rupture of blood vessels and is associated with erythropoietic and mesenchymal cell death. *Cell* 38: 597–607, 1984. doi:10.1016/0092-8674(84)90514-2.
32. **Pepin M**, **Schwarze U**, **Superti-Furga A**, **Byers PH.** Clinical and genetic features of Ehlers-Danlos syndrome type IV, the vascular type. *N Engl J Med* 342: 673–680, 2000 [Erratum in *N Engl J Med* 344: 392, 2001] doi:10.1056/NEJM200003093421001.
33. **Rahkonen O**, **Su M**, **Hakovirta H**, **Koskivirta I**, **Hormuzdi SG**, **Vuorio E**, **Bornstein P**, **Penttinen R.** Mice with a deletion in the first intron of the Col1a1 gene develop age-dependent aortic dissection and rupture. *Circ Res* 94: 83–90, 2004. doi:10.1161/01.RES.0000108263.74520.15.
34. **Xu J**, **Shi GP.** Vascular wall extracellular matrix proteins and vascular diseases. *Biochim Biophys Acta* 1842: 2106–2119, 2014. doi:10.1016/j.bbadis.2014.07.008.